

LETTER TO THE EDITOR

The evolutionary state of the southern dense core Chamaeleon-MMS1

A. Belloche¹, B. Parise¹, F. F. S. van der Tak^{1,*}, P. Schilke¹, S. Leurini¹, R. Güsten¹, and L.-Å. Nyman²

¹ Max-Planck-Institut für Radioastronomie, Auf dem Hügel 69, 53121 Bonn, Germany
e-mail: belloche@mpi.fr-bonn.mpg.de

² European Southern Observatory, Alonso de Cordova 3107, Casilla 19001, Santiago 19, Chile

Received 29 March 2006; Accepted 18 May 2006

ABSTRACT

Aims. Our goal is to set constraints on the evolutionary state of the dense core Cha-MMS1 in the Chamaeleon I molecular cloud.

Methods. We analyze molecular line observations carried out with the new submillimeter telescope APEX. We look for outflow signatures around the dense core and probe its chemical structure, which we compare to predictions of models of gas-phase chemistry. We also use the public database of the Spitzer Space Telescope (SST) to compare Cha-MMS1 with the two Class 0 protostars IRAM 04191 and L1521F, which are at the same distance.

Results. We measure a large deuterium fractionation for N_2H^+ ($11 \pm 3\%$), intermediate between the prestellar core L1544 and the very young Class 0 protostar L1521F. It is larger than for HCO^+ ($2.5 \pm 0.9\%$), which is probably the result of depletion removing HCO^+ from the high-density inner region. Our CO(3-2) map reveals the presence of a bipolar outflow driven by the Class I protostar Ced 110 IRS 4 but we do not find evidence for an outflow powered by Cha-MMS1. We also report the detection of Cha-MMS1 at 24, 70 and 160 μm by the instrument MIPS of the SST, at a level nearly an order of magnitude lower than IRAM 04191 and L1521F.

Conclusions. Cha-MMS1 appears to have already formed a compact object, either the first hydrostatic core at the very end of the prestellar phase, or an extremely young protostar that has not yet powered any outflow, at the very beginning of the Class 0 accretion phase.

Key words. stars: formation – ISM: individual objects: Cha-MMS1 – ISM: abundances – astrochemistry – ISM: jets and outflows

1. Introduction

The study of the earliest phases of star formation, the so-called prestellar and Class 0 stages, is essential to understand the origin of the stellar initial mass function (e.g. Ward-Thompson et al. 2006). As one of the closest active sites of low-mass star formation, the Chamaeleon I dark cloud is an excellent target to make progress in this field. However, its population of prestellar cores is not known and only 1 or 2 Class 0 protostellar *candidates* have been reported so far (see Reipurth et al. 1996; Froebrich 2005). The most promising of them, Cha-MMS1, is embedded in a $C^{18}O(1-0)$ clump (Haikala et al. 2005), in the Cederblad 110 region where several young stellar objects have been identified in the infrared (e.g. Prusti et al. 1991; Persi et al. 2001). Using a *tentative* far-infrared detection, Lehtinen et al. (2001) derived a low temperature ($T_{bol} = 20$ K) and luminosity ($L_{bol} = 0.45 L_{\odot}$) for Cha-MMS1. They proposed that it is a Class 0 protostar, in agreement with Reipurth et al. (1996) who suggested that it could be the driving source of the Herbig-Haro objects and the CO outflow seen nearby. However Lehtinen et al. (2003) failed to detect cm-wave emission with the ATCA interferometer, suggesting it is still prestellar. Here, in an effort to clarify its evolutionary state, we report molecular line observations carried out with the new submillimeter telescope APEX¹ and the infrared

detection of Cha-MMS1 at 24, 70 and 160 μm by the Spitzer Space Telescope.

2. Observations

We observed the dense core Cha-MMS1 ($\alpha_{2000} = 11^h06^m31^s.7$, $\delta_{2000} = -77^{\circ}23'33''$, Reipurth et al. 1996) in July, September and November 2005 with the APEX telescope (Güsten et al., this volume). The double-side-band heterodyne receiver APEX-2A (Risacher et al., this volume) was tuned to the molecular transitions listed in Table 2. The $N_2H^+(4-3)$ line was observed simultaneously with the H_2D^+ line in the 1 GHz bandpass. The half-power beamwidth was $18''$ at 345 GHz, and the forward and beam efficiencies used to convert antenna temperatures T_a^* into main-beam temperatures T_{mb} were 0.97 and 0.73, respectively. The double-side-band system temperatures (continuum calibration) ranged from 100 to 360 K in T_a^* scale. From spectra taken on different days, we estimate the calibration uncertainty better than $\sim 15\%$. The backend was a Fast-Fourier-Transform spectrometer with 16384 channels and a channel spacing of 61 kHz yielding an effective spectral resolution of about 120 kHz (Klein et al., this volume). The telescope pointing was checked on R-Dor, 07454-7112, IRAS 15194-5115, or Mars and found to be accurate to $\sim 4''$ (rms). The telescope focus was optimized on Saturn or Mars. The observations were performed in position-switching mode using the APECS software (Muders et al., this volume). The data were reduced with the CLASS software (see <http://www.iram.fr/IRAMFR/GILDAS>).

* Present address: SRON, 9747 AD Groningen, The Netherlands

¹ This publication is based on data acquired with the Atacama Pathfinder Experiment (APEX). APEX is a collaboration between the Max-Planck-Institut für Radioastronomie, the European Southern Observatory, and the Onsala Space Observatory.

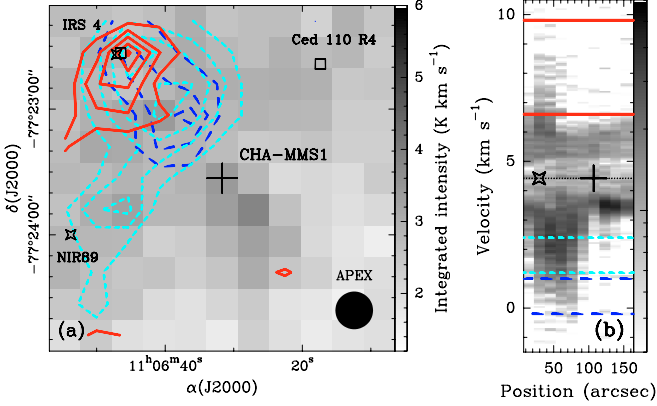


Fig. 1. **a)** CO(3-2) integrated intensity observed with APEX toward Cha-MMS1 (*cross*). The emission integrated over $[3.6, 5.8]$ km s⁻¹ is shown in greyscale. The blueshifted, less blueshifted and redshifted emissions integrated over $[-0.2, 1.0]$, $[1.2, 2.4]$ and $[6.6, 9.8]$ km s⁻¹ are plotted as long-dashed, short-dashed and thick contours, respectively. The steps are 3σ , 6σ and 3σ with rms $\sigma = 0.13, 0.13$ and 0.24 K km s⁻¹, respectively. The HPBW is shown on the right. The star and square symbols mark the position of near-infrared (Persi et al. 2001) and 3.5 cm sources (Lehtinen et al. 2003). **b)** CO(3-2) position-velocity diagram along the axis going through IRS 4 and Cha-MMS1. The dotted line indicates the systemic velocity of Cha-MMS1. The other lines show the limits of the velocity ranges used for the contour maps. The logarithmic temperature scale varies from 0.3 to 6 K.

3. Analysis: kinematics and deuteration

3.1. No evidence for an outflow driven by Cha-MMS1

We mapped the region around Cha-MMS1 in CO(3-2) with a spacing of 15". The spectra are deeply self-absorbed. They are very broad with stronger wing emission in the northeastern part. Figure 1a shows maps of the emission integrated over the core and the wings of the line. The blueshifted and redshifted emissions are clearly associated with the Class I protostar Ced 110 IRS 4 and very likely trace a bipolar outflow. Their morphology and the position-velocity diagram shown in Fig. 1b fall into case 1 of Cabrit & Bertout (1990), which suggests that the outflow axis is close to the line of sight ($i \lesssim 30^\circ$). The outflow geometry is consistent with the geometry of the bipolar nebula seen in the near infrared around IRS 4 (Zinnecker et al. 1999). The emission integrated over less blueshifted velocities traces the same lobe close to IRS 4 but in addition shows a prominent extension toward the near-infrared source NIR89, a potential Class I young brown dwarf (Persi et al. 2001). This additional wing emission could be associated with another outflow driven by NIR89, since Prusti et al. (1991) detected an elongated redshifted emission in CO(1-0) on the other side of NIR89 (see their Fig. 5). This potential second outflow would have an intermediate inclination ($20^\circ \lesssim i \lesssim 70^\circ$) since its two lobes do not overlap. On the other hand, we do not find significant wing emission in the vicinity of Cha-MMS1, which indicates that it does not drive an outflow on the scale probed with APEX.

3.2. Physical structure of Cha-MMS1

We derive the density structure of Cha-MMS1 from 1.3 mm continuum measurements done with SEST (Reipurth et al. 1996). Assuming a uniform dust temperature of 10 K, optically thin emission and a dust opacity $\kappa_{1.3\text{mm}} = 0.01$ cm² g⁻¹ (van der Tak et al. 1999), we derive a mass of $0.40 M_\odot$ in the 22" SEST beam and $1.0 M_\odot$ in the region within the 5σ contour level of

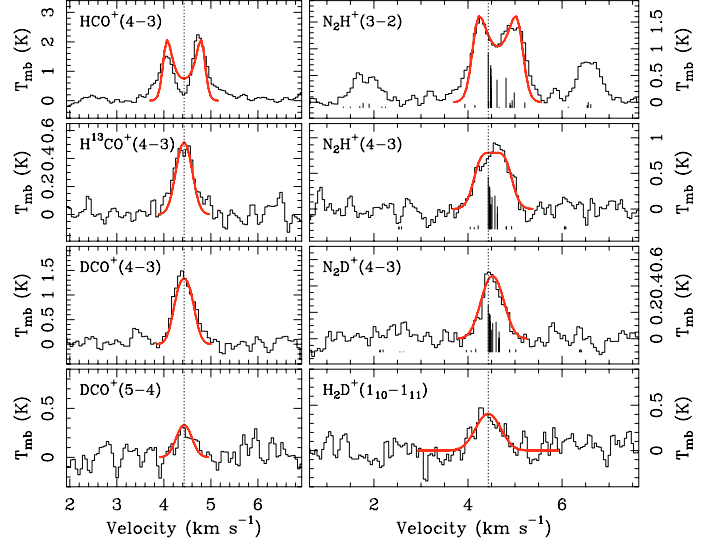


Fig. 2. Spectra observed with APEX toward Cha-MMS1 (*histogram*). Synthetic spectra corresponding to the model of Sect. 3.3 are superimposed (*thick line*). The hyperfine structure of the N₂H⁺ and N₂D⁺ lines is shown under each spectrum with statistical weighting. The dotted line indicates the systemic velocity assumed for the modeling.

Reipurth et al. (1996), which has a deconvolved diameter of $\sim 32''$. If the dense core has a flat inner region and a density decreasing as r^{-2} , which is typical for prestellar condensations (e.g. Bacmann et al. 2000), then the two measurements yield a central density $n_{\text{H}_2, \text{c}} = 3.3^{+0.4}_{-0.6} \times 10^6$ cm⁻³ and a radius of the flat inner region $r_{\text{flat}} = 1800^{+450}_{-200}$ AU at a distance of 150 pc (Knude & Høeg 1998).

3.3. Molecular abundances and deuteration

The spectra obtained with APEX toward the continuum peak position of Cha-MMS1 are presented in Fig. 2 and the results of single Gaussian and 7-component HFS fits done with the CLASS software are written in Table 1. The systemic velocities derived from the fits agree quite well except for N₂H⁺(4-3) and H₂D⁺(1₁₀-1₁₁). Since these two lines were observed simultaneously in the same bandpass, we suspect an instrumental problem and have shifted these two spectra by -0.20 MHz in Fig. 2 to compensate for this difference. In the following, we assume a systemic velocity of 4.43 km s⁻¹. The opacity of N₂D⁺(4-3) is small and hence not well constrained by the HFS fit. We fixed it to 0.5 (see model below). The opacity of N₂H⁺(3-2) is also uncertain, although this is not seen in the statistical uncertainty². Assuming a kinetic temperature of 10 K, the non-thermal linewidths are between ~ 0.4 and ~ 0.5 km s⁻¹. The linewidths derived from the HFS fits should not be affected by optical depth effects. They agree with each other within 2σ and we find a weighted mean $\Delta V_{\text{NT}} = 0.40 \pm 0.02$ km s⁻¹. This corresponds to a non-thermal dispersion $\sigma_{\text{NT}} = 0.17 \pm 0.01$ km s⁻¹ which is on the same order as the thermal velocity dispersion at 10 K. There is therefore a significant amount of non-thermal motions in the dense core.

The HCO⁺(4-3) spectrum is strongly self-absorbed and asymmetric, the red peak being stronger than the blue one, and

² The self-absorption of the central group of hyperfine components lowers its “mean peak temperature” and the opacity derived by the HFS fit is then artificially increased. For test purposes, we masked out the self-absorption and the opacity was reduced to 19.6 ± 1.1 .

Table 1. Results of single Gaussian (*top*) and 7-component HFS (*bottom*) fits to the spectra observed toward the center of Cha-MMS1.

Line	$V_{\text{lsr}}^{(1)}$ (km s ⁻¹)	$FWHM^{(1)}$ (km s ⁻¹)	$Area^{(1)}$ (K km s ⁻¹)	T_a^* (K)	rms (mK)	$\Delta V_{\text{NT}}^{(1,2)}$ (km s ⁻¹)
H ¹³ CO ⁺ (4-3)	4.42(8)	0.53(3)	0.20(1)	0.35	41	0.53(3)
DCO ⁺ (4-3)	4.42(1)	0.51(3)	0.58(3)	1.08	90	0.49(3)
DCO ⁺ (5-4)	4.47(4)	0.46(8)	0.095(15)	0.20	71	0.44(8)
H ₂ D ⁺ (₁₁₀₋₁₁₁)	4.57(4)	0.63(7)	0.20(2)	0.31	78	0.53(8)

Line	$V_{\text{lsr}}^{(1)}$ (km s ⁻¹)	$FWHM^{(1)}$ (km s ⁻¹)	$T_a^* \times \tau_{\text{tot}}^{(1)}$ (K)	$\tau_{\text{tot}}^{(1)}$ (K)	rms (mK)	$\Delta V_{\text{NT}}^{(1,2)}$ (km s ⁻¹)
N ₂ H ⁺ (3-2)	4.44(1)	0.42(1)	24(2)	24(2)	50	0.40(1)
N ₂ H ⁺ (4-3)	4.65(2)	0.50(5)	2.3(7)	3.4(14)	81	0.49(5)
N ₂ D ⁺ (4-3)	4.44(2)	0.41(3)	0.53(3)	0.5(0)	44	0.40(3)

(1) The statistical uncertainties in parenthesis are given in units of the last digit. 0 means the parameter was fixed. For V_{lsr} , they include the contribution of the frequency uncertainties listed in Table 2.

(2) The non-thermal linewidth was computed assuming $T_K = 10$ K and, for the Gaussian fits, optically thin emission.

the low-optical depth H¹³CO⁺(4-3) line peaks in between. The asymmetry of the HCO⁺(4-3) line actually changes across our small map: the blue peak is stronger than the red one in the southern part below (0, -10''). This pattern could result from rotation (e.g. Redman et al. 2004) or a combination of infall and rotation, provided the actual center of the core is slightly offset from our ‘‘central’’ position toward the South (by ~5''). However we did not detect a clear overall velocity gradient in our N₂H⁺(4-3) map over 50'' that would unambiguously reveal the presence of rotation.

We used the Monte-Carlo-based radiative-transfer code MAPYSO (see Belloche et al. 2002 and references therein) to model the emission in HCO⁺, H¹³CO⁺, DCO⁺, N₂H⁺ and N₂D⁺. For all species, we used the collision rates of HCO⁺ with H₂ (Flower 1999). We modeled the N₂H⁺ and N₂D⁺ lines as simple lines, without the hyperfine structure. The H₂D⁺ emission was modeled with the Monte-Carlo program RATRAN (see Hogerheijde & van der Tak 2000). We used the density profile described in Sect. 3.2 and the velocity was set to zero. We assumed uniform gas temperature, abundance and non-thermal broadening for each molecule. We fixed the isotopic ratio $\frac{[\text{HCO}^+]}{[\text{H}^{13}\text{CO}^+]}$ to 70.

The synthetic spectra of the best-fit model are overlaid in Fig. 2 and the parameters are shown in Table 2. The total opacities that we estimate from τ_{peak} using the statistical weights agree well with the opacities derived from the 7-component HFS fits (see Table 1 and Footnote 2). The non-thermal broadening derived for HCO⁺ and its isotopologues is more reliable than the one *measured* in Table 1 because the opacity broadening is properly taken into account in the modeling. On the other hand, it is less reliable for N₂H⁺ and N₂D⁺ since part of it mimics the broadening by the hyperfine structure not implemented in our model. The non-thermal broadening derived for H₂D⁺ is larger than for HCO⁺ and its isotopologues, but given the low signal-to-noise ratio of the H₂D⁺ spectrum, it may not be significant. The one *measured* for N₂H⁺ and N₂D⁺ in Table 1 lies in between. From the abundances obtained in Table 2 we derive the following deuterium fractionations: $\frac{[\text{N}_2\text{D}^+]}{[\text{N}_2\text{H}^+]} = 11 \pm 3\%$ and $\frac{[\text{DCO}^+]}{[\text{HCO}^+]} = 2.5 \pm 0.9\%$. The deuterium fractionation is therefore ~4 times larger for N₂H⁺ than for HCO⁺.

Table 2. Gas temperature, non-thermal broadening and abundance of each molecule for the best-fit model. The peak opacity of each modeled transition is also given, as well as an estimation of the total opacity of the hyperfine multiplets if they had been modeled.

Molec.	Line	Frequency ⁽¹⁾ (MHz)	T_k (K)	ΔV_{NT} (km s ⁻¹)	χ^2 ⁽²⁾	τ_{peak}	τ_{tot}
HCO ⁺	4-3	356734.134(50)	8.8	0.35	8.4(-10)	44	-
H ¹³ CO ⁺	4-3	346998.338(89)	8.8	0.35	1.2(-11)	0.46	-
DCO ⁺	4-3	288143.858(7)	8.8	0.35	2.1(-11)	1.2	-
	5-4	360169.778(7)				0.25	-
N ₂ H ⁺	3-2	279511.858(11)	7.3	0.50	2.2(-10)	15	16
	4-3	372672.560(13)				3.4	3.6
N ₂ D ⁺	4-3	308422.322(10)	7.3	0.50	2.5(-11)	0.49	0.51
o-H ₂ D ⁺	₁₁₀₋₁₁₁	372421.385(10)	8	0.50	4.3(-11)	0.19	-

(1) from the CDMS catalog as of Feb. 2006 (see Müller et al. 2005). The uncertainties in parenthesis are given in units of the last digit.

(2) $X(p)$ means $X \times 10^p$.

4. Implications: evolutionary state of Cha-MMS1

The deuterium fractionations of HCO⁺ and N₂H⁺ derived in Sect. 3.3 are 3-4 orders of magnitude larger than the cosmic ratio $\frac{[\text{D}]}{[\text{H}]} \sim 10^{-5}$. This enhanced molecular deuteration is typical for low-mass dense cores (e.g. Williams et al. 1998; Crapsi et al. 2005; Parise et al. 2006) and correlates well with CO depletion in prestellar cores (Bacmann et al. 2003). It is understood as a result of CO freeze out onto the grain surface, CO being the major destroyer of H₂D⁺, the key ion in the molecular deuterium chemistry (e.g. Caselli et al. 2003). To understand the different deuteration degrees measured for HCO⁺ and N₂H⁺ in Cha-MMS1, we compare our results with the predictions of chemical models. Roueff et al. (2005) calculated the steady state of models of gas-phase chemistry at 10 K. Their three models, Model 1, 2, and 3, have densities of 10⁴, 10⁵, and 10⁶ cm⁻³, and C and O depletion factors of 1, 5, and 15, respectively. At 10 K, the ortho-to-para ratio of H₂D⁺ is close to 1 (Gerlich et al. 2002), so we deduce a total H₂D⁺ abundance of $\sim 9 \times 10^{-11}$, in agreement with Model 3 and close to the value derived for the evolved prestellar core L1544 (van der Tak 2006). For N₂H⁺, both the abundance and the deuterium fractionation in Table 2 agree well with the predictions of Model 3, while they are close to Model 2 for HCO⁺. The degree of deuterium fractionation in HCO⁺ traces therefore lower densities than the N₂H⁺ one. This can be understood if HCO⁺ is depleted at high densities, which is expected in dense cores since HCO⁺ is chemically related to CO. To test this scenario, we computed a model for HCO⁺ and isotopologues with a hole of radius 1800 AU and abundances 2.5 times larger: the fit to the observed spectra was as good as for the model shown in Fig. 2, suggesting that HCO⁺ may indeed be depleted in the inner region. Crapsi et al. (2005) derived a N₂H⁺ deuterium fractionation of 16–23% for L1544 and 5–10% for L1521F, which is now known as a Class 0 protostar since its detection by the Spitzer Space Telescope (SST) in the near infrared (e.g. Terebey et al. 2005). Our value for Cha-MMS1 lies in between, which suggests an evolutionary state between L1544 and L1521F if the $\frac{[\text{N}_2\text{D}^+]}{[\text{N}_2\text{H}^+]}$ ratio can be used as a chemical clock.

The higher spatial resolution provided by APEX and the higher densities traced by CO(3-2) allowed us to resolve the blueshifted wing emission seen earlier in CO(1-0) (Mattila et al. 1989; Prusti et al. 1991) into two outflows – the second one

being tentative –, and assign their driving sources. The main outflow is *not* powered by Cha-MMS1, as Reipurth et al. (1996) suggested, but by the Class I protostar Ced 110 IRS 4. This is consistent with the non-detection of Cha-MMS1 in centimeter continuum emission (Lehtinen et al. 2003). Since we did not find evidence for an outflow driven by Cha-MMS1 itself, the dense core must be in an earlier evolutionary state than the typical young Class 0 protostar IRAM 04191 which does have a powerful outflow (André et al. 1999). However, using the SST archive (<http://ssc.spitzer.caltech.edu/>), we discovered a source detected at 24, 70 and 160 μm by the instrument MIPS (PID:37, REQID:3962112), offset from Cha-MMS1 by 5–7'' toward the East. Given the large beams of SEST (22'') and SST (6–18'') and their pointing rms accuracies (3'' and 1.4'', respectively), we find it conceivable that this mid-infrared source is embedded in the Cha-MMS1 dense core. We measure fluxes of 2.5 ± 0.8 and 200 ± 100 mJy at 24 and 70 μm . The 24 μm flux is ~ 7 and 10 times smaller than the fluxes we measured for IRAM 04191 and L1521F using the SST data products of the C2D legacy program (Evans et al. 2003), and the 70 μm flux ~ 4 and 3 times smaller³. In addition, Cha-MMS1 was not detected at 8 μm by the instrument IRAC (SST public data, PID:37, REQID:3960320), at a 3σ level ~ 9 and 7 times lower than the peak fluxes of IRAM 04191 and L1521F. The detection at 24 μm implies that Cha-MMS1 already contains a compact hydrostatic object (e.g. Masunaga & Inutsuka 2000), but the weakness and “redder” color of the 24 and 70 μm fluxes and the non-detection at 8 μm suggest that it is less evolved than IRAM 04191 and L1521F (e.g. Young & Evans 2005), since they are at the same distance. Depending on its inclination along the line of sight (see Boss & Yorke 1995; Whitney et al. 2003, for its effects on the mid-infrared fluxes), it could be at the stage of the first hydrostatic core, i.e. at the very end of the prestellar phase, or have already formed an extremely young Class 0 protostar that has not yet powered any outflow. At a stage intermediate between L1544 and L1521F, Cha-MMS1 would then be the first object found so close to the very beginning of the Class 0 accretion phase.

Acknowledgements. We thank P. André and J. Kauffmann for enlightening discussions about Cha-MMS1 and the SST, and the APEX staff for their help during the observations. BP is grateful to the A. von Humboldt Foundation for a Humboldt Research Fellowship.

References

- André, P., Motte, F., & Bacmann, A. 1999, *ApJ*, 513, L57
 Bacmann, A., André, P., Puget, J.-L., Abergel, A., Bontemps, S., & Ward-Thompson, D. 2000, *A&A*, 361, 555
 Bacmann, A., Lefloch, B., Ceccarelli, C., Steinacker, J., Castets, A., & Loinard, L. 2003, *ApJ*, 585, L55
 Belloche, A., André, P., Despois, D., & Blinder, S. 2002, *A&A*, 393, 927
 Boss, A. P., & Yorke, H. W. 1995, *ApJ*, 439, L55
 Cabrit, S., & Bertout, C. 1990, *ApJ*, 348, 530
 Caselli, P., van der Tak, F. F. S., Ceccarelli, C., & Bacmann, A. 2003, *A&A*, 403, L37
 Crapsi, A., Caselli, P., Walmsley, C. M., Myers, P. C., Tafalla, M., Lee, C. W., & Bourke, T. L. 2005, *ApJ*, 619, 379
 Evans, N. J., II, Allen, L. E., Blake, G. A., et al. 2003, *PASP*, 115, 965
 Flower, D. R. 1999, *MNRAS*, 305, 651
 Froebrich, D. 2005, *ApJS*, 156, 169
 Gerlich, D., Herbst, E., & Roueff, E. 2002, *Planet. Space Sci.*, 50, 1275
 Haikala, L. K., Harju, J., Mattila, K., & Toriseva, M. 2005, *A&A*, 431, 149
 Hogerheijde, M.R., & van der Tak, F.F.S. 2000, *A&A*, 362, 697
 Knude, J., & Høg, E. 1998, *A&A*, 338, 897
 Lehtinen, K., Haikala, L. K., Mattila, K., & Lemke, D. 2001, *A&A*, 367, 311
 Lehtinen, K., Harju, J., Kontinen, S., & Higdón, J. L. 2003, *A&A*, 401, 1017
 Mattila, K., Liljestrom, T., & Toriseva, M. 1989, in *Low Mass Star Formation and Pre-main Sequence Objects*, Ed. B. Reipurth, ESO Conf. Workshop Proc., 33, 153
 Masunaga, H., & Inutsuka, S.-I. 2000, *ApJ*, 531, 350
 Müller, H. S. P., Schlöder, F., Stutzki, J., & Winnewisser, G. 2005, *J. Mol. Struct.*, 742, 215
 Parise, B., Ceccarelli, C., Tielens, A.G.G.M., Castets, A., Caux, E., Lefloch, B., & Maret, S. 2006, *A&A*, *in press*
 Persi, P., Marenzi, A. R., Gómez, M., & Olofsson, G. 2001, *A&A*, 376, 907
 Prusti, T., Clark, F. O., Whittet, D. C. B., Laureijs, R. J., & Zhang, C. Y. 1991, *MNRAS*, 251, 303
 Redman, M. P., Keto, E., Rawlings, J. M. C., & Williams, D. A. 2004, *MNRAS*, 352, 1365
 Reipurth, B., Nyman, L.-Å., & Chini, R. 1996, *A&A*, 314, 258
 Roueff, E., Lis, D. C., van der Tak, F. F. S., Gerin, M., & Goldsmith, P. F. 2005, *A&A*, 438, 585
 Terebey, S., Sullivan, A., Fich, M., & Padgett, D. L. 2005, *AAS Meet. Abstr.*, 207, 165.01
 Van der Tak, F. F. S., van Dishoeck, E. F., Evans, N. J., Bakker, E. J., & Blake, G. A. 1999, *ApJ*, 522, 991
 Van der Tak, F. F. S. 2006, *Phil. Trans. R. Soc. Lond. A*, *in press* [[astro-ph/0602340](http://arxiv.org/abs/astro-ph/0602340)]
 Ward-Thompson, D., André, P., Crutcher, R., et al. 2006, in *Protostars and planets V*, Ed. B. Reipurth, D. Jewitt & K. Keil (Tucson: Univ. Arizona Press), *in press*
 Whitney, B. A., Wood, K., Bjorkman, J. E., & Cohen, M. 2003, *ApJ*, 598, 1079
 Williams, J. P., Bergin, E. A., Caselli, P., Myers, P. C., & Plume, R. 1998, *ApJ*, 503, 689
 Young, C. H., & Evans, N. J. 2005, *ApJ*, 627, 293
 Zinnecker, H., Krabbe, A., McCaughrean, M. J., et al. 1999, *A&A*, 352, L73

³ Note that the 70 μm flux is one order of magnitude weaker than the questionable 3.7σ detection of Lehtinen et al. (2001) with ISOPHOT.